Fullerene functionalized halogen bonding heteroditopic hosts for ion-pair recognition

Krzysztof M. Bąk,† Igor Marques, Heike Kuhn, Kirsten E. Christensen, Vítor Félix,* and Paul D. Beer*

ABSTRACT: Despite their hydrophobic surfaces with localized π holes and rigid well-defined architectures providing a scaffold for preorganizing binding motifs, fullerenes remain unexplored as potential supramolecular host platforms for the recognition of anions. Herein, we present the first example of the rational design, synthesis, and unique recognition properties of novel fullerene-functionalized halogen bonding (XB) heteroditopic ion-pair receptors containing cation and anion binding domains spatially separated by C_{60}. Fullerene spatial separation of the XB donors and the crown ether complexed potassium cation resulted in a rare example of an artificial receptor containing two anion binding sites with opposing preferences for hard and soft halides. Importantly, the incorporation of the C_{60} motif into the heteroditopic receptor structure has a significant effect on halide binding selectivity, which is further amplified upon K^+ cation binding. The potassium cation complexed fullerene based receptors exhibit enhanced selectivity for the soft polarizable iodide ion which is assisted by the C_{60} scaffold preorganizing the potent XB-based binding domains, anion-π interactions and the exceptional polarizability of the fullerene moiety, as evidenced from computational DFT calculations. These observations serve to highlight the unique properties of fullerene surfaces for proximal charged guest binding with potential applications in construction of selective molecular sensors and modulating the properties of solar cell devices.

Introduction

Fullerenes are unique molecules with a large spherical surface, strong electron acceptor properties, high electric polarizability, and curved π-electron systems capable of forming noncovalent interactions with electron rich molecules.[1–13] As a result, they have been incorporated in numerous functional molecular assemblies and supramolecular arrays with a wide variety of applications in photochemistry, medicinal chemistry and organic electronics.[14–26] Although molecular electrostatic potential (MEP) surfaces of simple fullerenes are positive, surprisingly, their interaction with anions has been largely overlooked.[6,27] Only recently, Matile and co-workers demonstrated remarkable examples of the stabilization of anionic transition states in anion-π catalysis on a fullerene surface.[28–30] While Lei and co-workers reported facilitated charge transfer in solid state aggregates of self n-doped fullerene ammonium iodide, which is believed to be a result of iodide-C_{60} interactions.[31] However, thus far fullerene surfaces have not been exploited as potential supramolecular host platforms for the recognition of simple anions (e.g. halides) in molecular receptor structural design. Nevertheless, it is worth noting that an open-cage fullerene was demonstrated as a molecular container for F^-, Cl^-, Br^-, and I^-.[32]

The MEP surface of C_{60} reveals highly localized areas of positive potential – π-holes (Figure 1), which can be presumably used in anion recognition. Anion-π interactions are widely recognized and frequently exploited in the design of selective anion binding receptors.[33–36] Strong attraction between an anion and a π-system can be achieved by electron-withdrawing substituents that further polarize the molecule and lead to a positive quadrupole moment along the axis perpendicular to the π-system, increasing the depth of a π-hole.[33] Interestingly, fullerenes are known for their remarkable polarizability[37] which, in principle, may enable a significant enhancement of anion-π interactions by exposure to an external electric field, produced for example by a proximate anion (so-called dynamic contribution) or cation. Moreover, the well-defined bulky architecture of fullerenes provides a potential scaffold for preorganization of binding motifs and a hydrophobic shield, which can create a microenvironment that excludes solvent molecules and enhances strength of non-covalent interactions.[38,39] Due to these features C_{60} constitutes an exceptional and unexplored platform for the design and construction of heteroditopic ion-pair receptors with increased affinity and selectivity. The positive cooperativity associated with the simultaneous proximal binding of oppositely charged species has been crucial in augmenting the ion-pair binding properties of

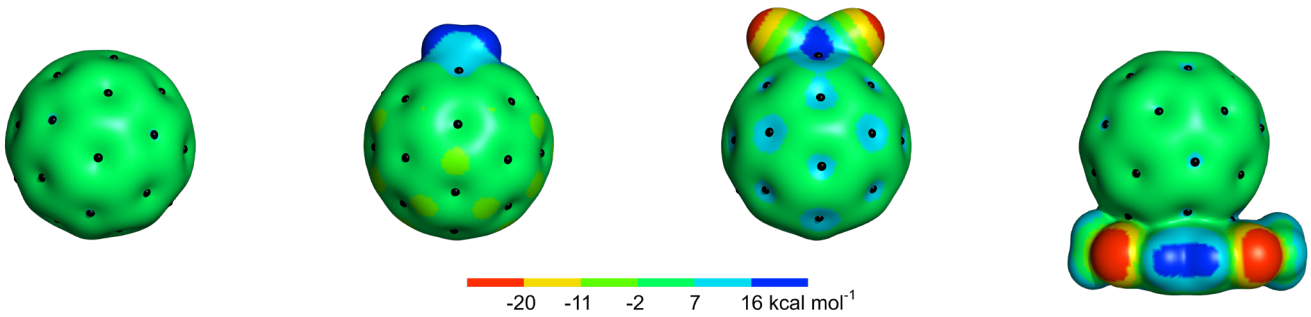

Figure 1. Molecular electrostatic potential (MEP) surface of C_{60} (left), C_{60} functionalized with methylene (centre left) or two cyano electron withdrawing groups (centre right), and C_{60} in association with naphthalene diimide (right). The π-holes on the surface of C_{60} are identified with black dots.

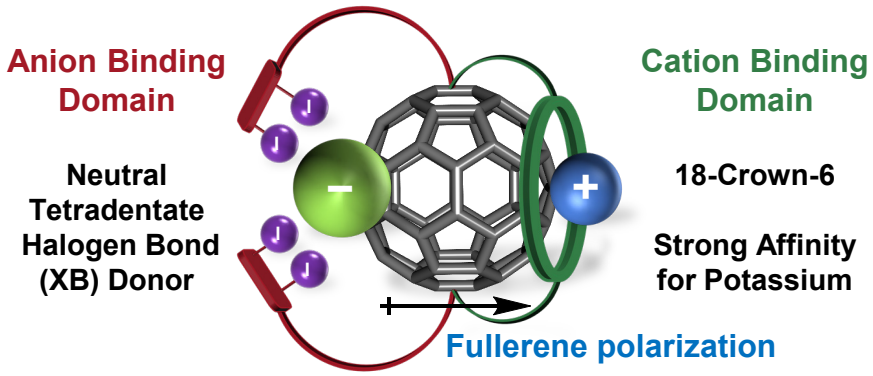

Figure 2. Cartoon representation of a tetradentate-XB fullerene functionalized heteroditopic host for ion-pair recognition. Purple spheres represent iodine halogen bond donors.

heteroditopic receptors relative to their monotopic receptor counterparts. As such, heteroditopic receptors have been increasingly employed in a myriad of applications including salt extraction and solubilisation,[40,41] membrane transport,[42,43] and biological zwitterion binding.[44,45]

The vast majority of reported heteroditopic receptors contain well-established recognition motifs such as crown ethers for cation recognition and hydrogen bond donors for anion complexation.[46–48] In recent years however, halogen bonding (XB), an interaction between a Lewis base and the σ-hole of an electron-deficient halogen atom, has emerged as a powerful addition to the anion supramolecular host-guest chemistry tool-box, due to its stringent linearity, comparable binding strength to hydrogen bonding (HB), and unique selectivity.[49–52] Herein, we describe for the first time the rational design, synthesis, and unique recognition properties of novel fullerene-functionalized halogen bonding heteroditopic ion-pair receptors containing cation and anion binding domains spatially separated by C_{60} (Figure 2).

Results and Discussion

Synthesis of fullerene heteroditopic ion-pair receptors. Interest in crown ether-fullerene adduct materials has been stimulated primarily by their photophysical, electrochemical and superconducting properties.[53] In particular, Echegoyen, Pretsch, Diederich and co-workers obtained the C_{60}-dibenzo-18-crown-6 (DB18C6) adduct in a highly regioselective double cyclopropanation (Bingel addition) taking place exclusively in the *trans-1* positions on the opposite poles of C_{60} (Figure 3a).[54,55] Potassium cation crown ether binding in proximity to the fullerene surface was shown to elicit significant perturbations of the fullerene host's reduction potentials, proving that alkali metal cation complexation can alter the physicochemical properties of C_{60}. We hypothesized that a complexed cation could further polarize the fullerene surface resulting in anion binding enhancement on the opposite size of the molecule (Figure 2). Therefore, we adapted the regioselective DB18C6 double Bingel fullerene addition for the synthesis of heteroditopic ion pair receptors **1** and **2** containing neutral acyclic XB donors based on 1,3-bis-(iodotriazole)nitroaryl motifs in the anion binding domains,[56] spatially separated from the polarizable fullerene surface by linkers of different lengths (Figure 3b).

The separate appropriately functionalized crown ether-fullerene cation and halogen bonding anion binding domain synthons were prepared according to Scheme 1 and Scheme 2 The synthesis of the bis-alkyne appended crown ether-

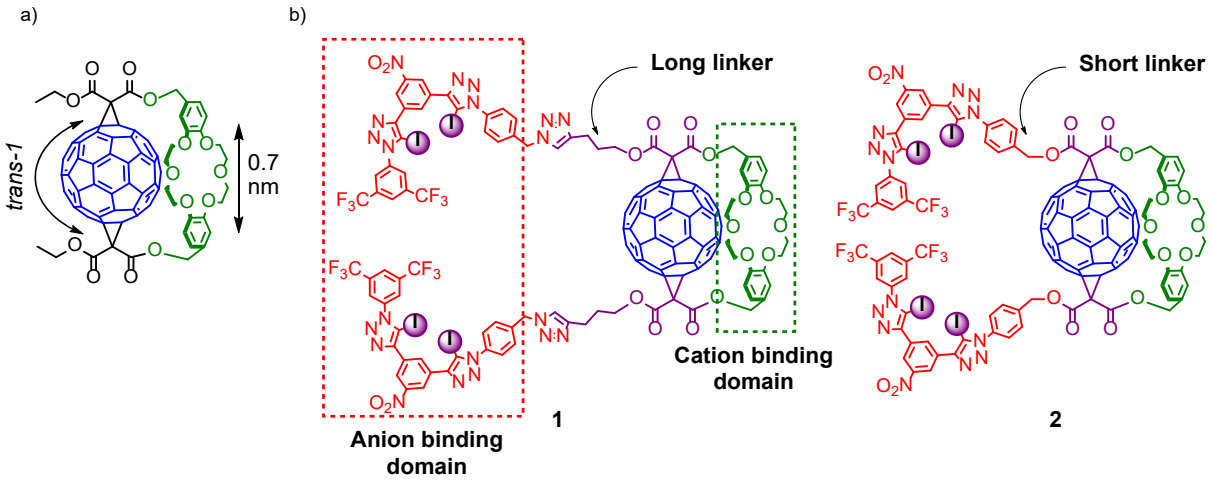

Figure 3. (a) C_{60}-Dibenzo-18-crown-6 adduct obtained by Echegoyen, Pretsch, Diederich and co-workers. (b) Heteroditopic ion pair receptors **1** and **2** with different linkers separating anion binding domains from C_{60} surface.

Scheme 1. Synthesis of C60-DB18C6 adduct 9. (a) $(ClCH_2)_2O$, K_2CO_3, DMF, 80°C, 36h, 21%; (b) K_2CO_3, DMF, 80°C, 24h, 31%; (c) $NaBH_4$, THF/MeOH 9:1, 0°C, 2h, 62%; (d) EDC·HCl, DMAP, KPF_6, CH_2Cl_2/CH_3CN 4:1, 0°C, 48h, 76%; (e) C_{60}, I_2, DBU, KPF_6, Toluene, RT, 6h, 25%.

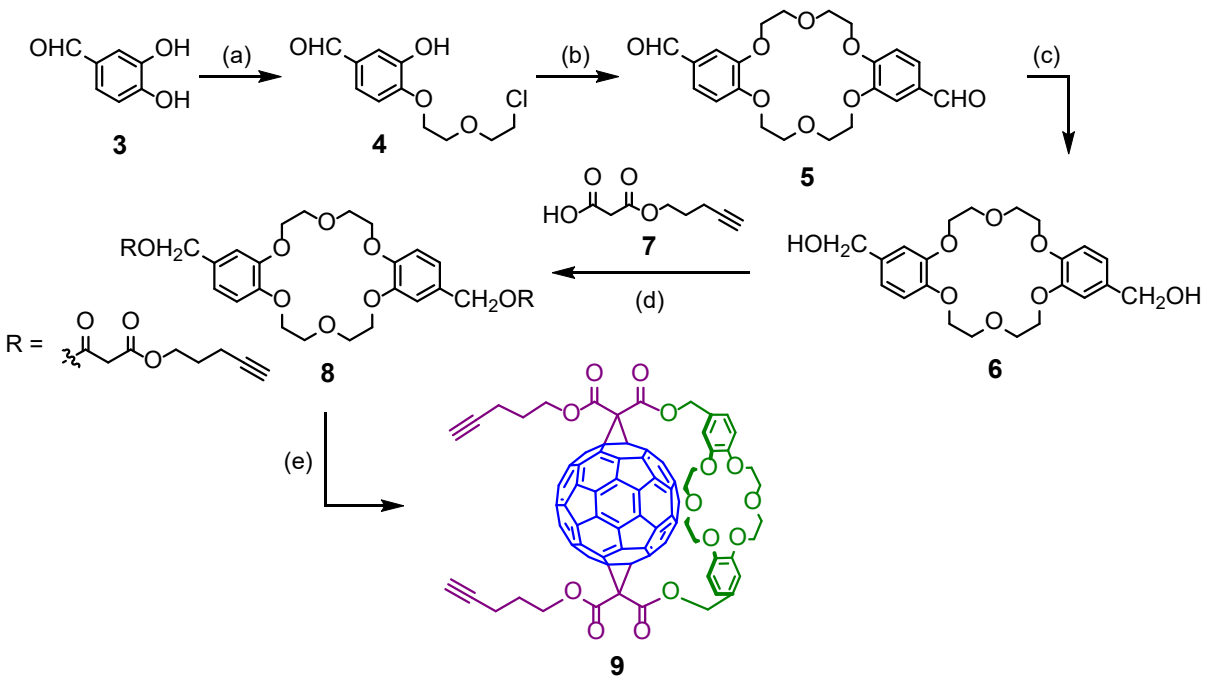

Scheme 2. Synthesis of anion binding domain and receptor 1. (a) $[Cu(CH_3CN)_4]PF_6$, TBTA, CH_2Cl_2, RT, 16h, 65%; (b) $[Cu(CH_3CN)_4]PF_6$, TBTA, CH_2Cl_2, RT, 16h 72%; (c) NaN_3, DMF, RT, 24h, 60%; (d) $[Cu(CH_3CN)_4]PF_6$, TBTA, CH_2Cl_2, RT, 48h, 36%.

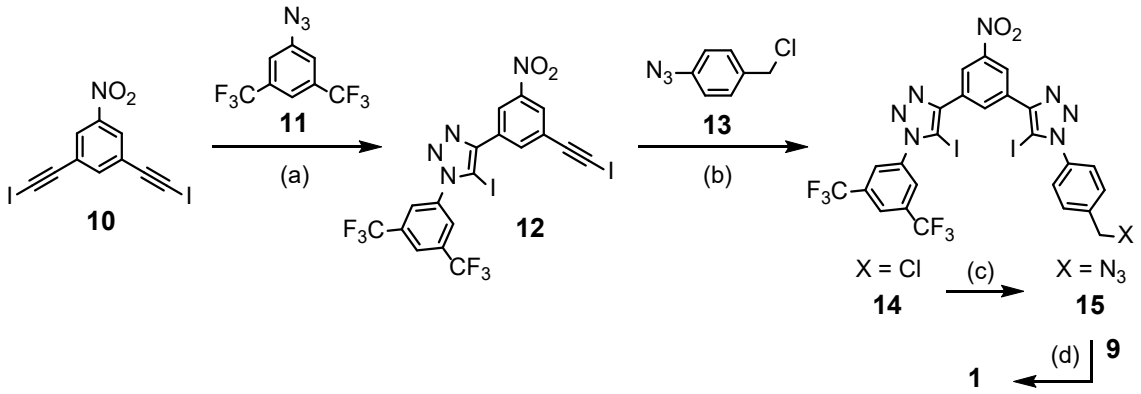

fullerene synthon **9** was achieved *via* modification of the regioselective procedure reported by Diederich and co-workers (Scheme 1).[54] 3,4-Dihydroxybenzaldehyde **3** was alkylated with an excess of bis(2-chloroethyl) ether to obtain **4** (21%), which could be readily separated from the other regioisomer. Macrocyclization of **4** in the presence of K^+ template afforded the poorly soluble *trans*-dialdehyde of DB18C6 **5** (31%), which upon reduction using $NaBH_4$ gave the diol **6** (62%). Mono-malonate **7** was prepared either by treating 4-pentyn-1-ol with Meldrum's acid (68%), or *via* an alternative approach involving selective mono-hydrolysis of a symmetric malonic ester (see ESI for details). Diol **6** was coupled with excess **7** using EDC to obtain bis-malonate ester crown ether **8** (76%). Bingel reaction of **8** with C_{60} in the presence of K^+ and I_2 led exclusively to the doubly substituted fullerene adduct **9** (25%). The ^1H NMR and ^{13}C NMR spectra of **9** were in agreement with *trans*-1 addition pattern (C_2 symmetry), which was later unambiguously confirmed by single crystal X-ray diffraction structural analysis (Figure 4).[57] Solid state analysis also revealed that the DB18C6 ester groups of the cyclopropane rings are situated on the same side of fullerene (out-out isomer). Interestingly, rotation of the crown ether moiety is significantly limited causing planar chirality and splitting of the benzylic and ether CH_2 signals in the ^1H NMR spectrum (see ESI).

The synthesis of the azide functionalized XB anion binding domain **15** required desymmetrization of bis-iodoalkyne building block **10** (Scheme 2). An excess of **10** was treated

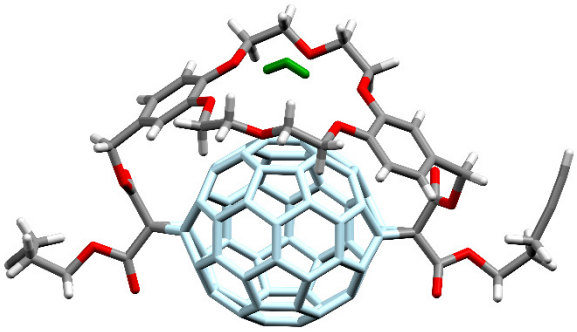

Figure 4. Solid-state structure of C_{60}-DB18C6 adduct **9** with a water molecule (green color) hydrogen bonded to crown ether.

with azide **11** in the presence of $[Cu(MeCN)_4]PF_6$ and Cu(I) stabilizing ligand TBTA to obtain mono-iodotriazole **12** (65%). It was then reacted with azide **13** to obtain asymmetric bis-iodotriazole **14** (72%), which could be readily transformed into azide **15** (60%). In the final step the anion binding moiety was doubly "clicked" with bis-alkyne crown ether fullerene adduct **9** to obtain ion-pair receptor **1** following purification by a flash and size-exclusion chromatography (36%).

The synthesis of receptor **2** with a shorter linker between the anion binding domain and a fullerene surface was initially attempted in an alternative approach with a Bingel reaction conducted on precursor **16** (Scheme 3). Unfortunately, this resulted in a complex mixture of products suggesting that the anion binding motif is not compatible with the conditions of the cyclopropanation. An alternative route involving Cu(I)-catalyzed azide–alkyne cycloaddition

Scheme 3. Different approaches to the synthesis of receptor 2. (a) C_{60}, I_2, DBU, KPF_6, Toluene, RT, 1h; (b) $[Cu(CH_3CN)_4]PF6$, TBTA, CH_2Cl_2, RT, 18h, 14%.

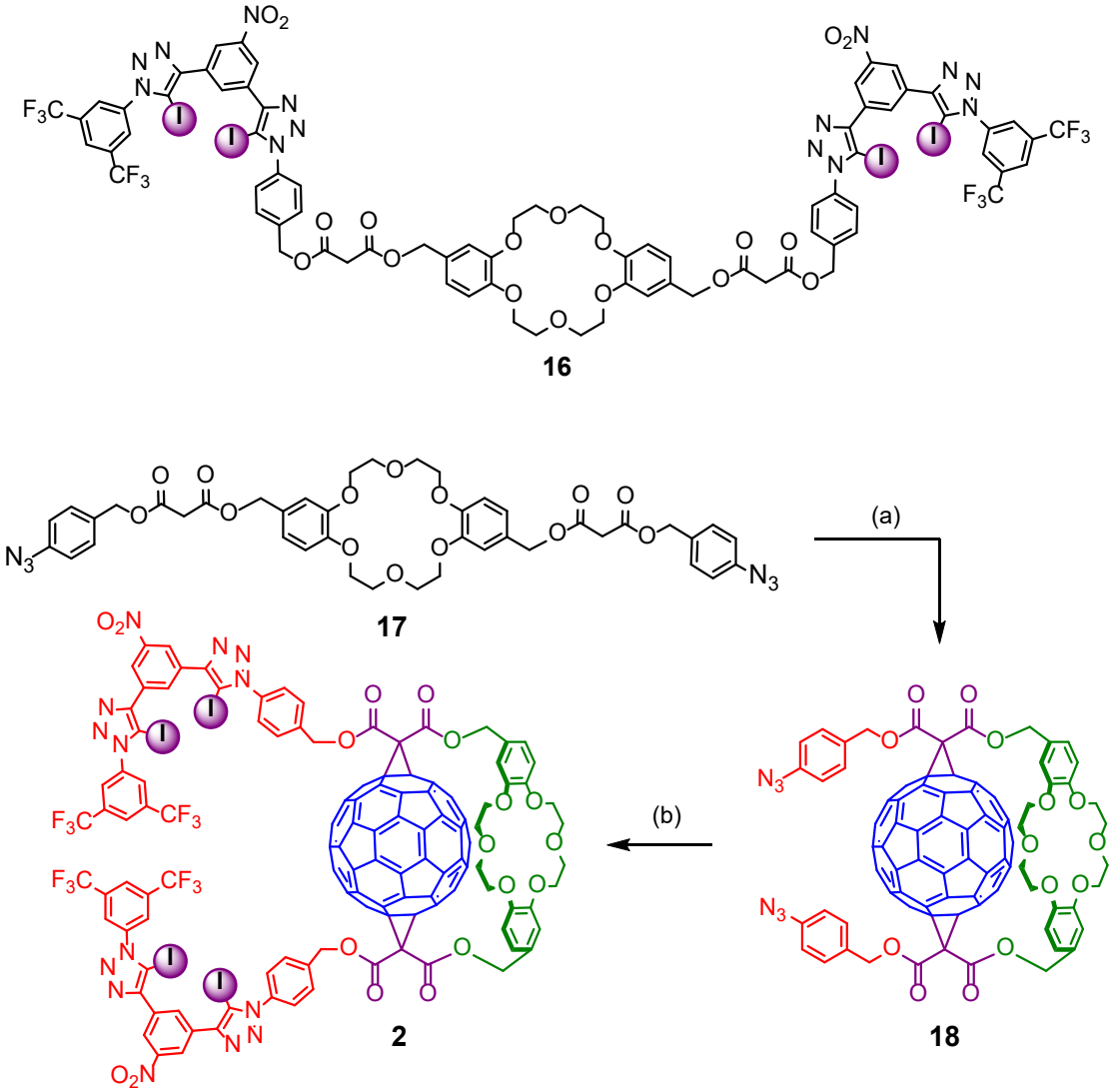

(CuAAC) reaction between alkyne **12** and DB18C6-fullerene bis-azide **18** proved successful (Scheme 3).Fullerene azides are known to be highly unstable due to possible reactions at the fullerene surface.[58–60] However, a Bingel reaction of short duration time between **17** and C_{60}, followed by rapid chromatographic purification afforded **18**, which was used immediately in the next step to obtain final receptor **2** (14%).

Anion and ion-pair binding studies. The anion binding properties of fullerene containing heteroditopic receptors **1** and **2** were investigated by ^{1}H NMR titration experiments in 3:1 $CDCl_3$:CD_3CN. Addition of TBA halides (Cl^-, Br^-, I^-) to solutions of the free receptors **1** or **2** caused significant shifts of the XB anion binding domain proton signals and no changes ($\Delta\delta$ < 0.01 ppm) of the crown ether cation binding protons were observed. Such a behavior strongly indicates that the ditopic binding domains of the receptors **1** and **2** are electronically and spatially well-separated from each other. Notably, the respective receptor's internal nitro-aryl proton *(a)* shifted downfield, which is indicative of halide binding in a cavity formed by the iodotriazole XB-donors (Figure 5). Bindfit analysis of the titration isotherm data revealed that 1:1 and 1:2 stoichiometric host-guest complexes are formed (Table 1). In the 1:1 complex, the halide anion is most likely bound by both bidentate XB motifs contributing up to four halogen bond donors. Upon addition of excess halide anion, each appended XB bidentate recognition site binds an individual anion with two halogen bond donors to form a 1:2 stoichiometric host-guest complex. Unsurprisingly then, $K_{1:1}$ association constant values are more than an order of magnitude larger than those of $K_{1:2}$. Receptor **1** binds halides more strongly than **2** with a selectivity trend Br^- > I^- > Cl^-. The enhanced halide anion binding by **1** may be attributed to the longer, flexible linker providing the

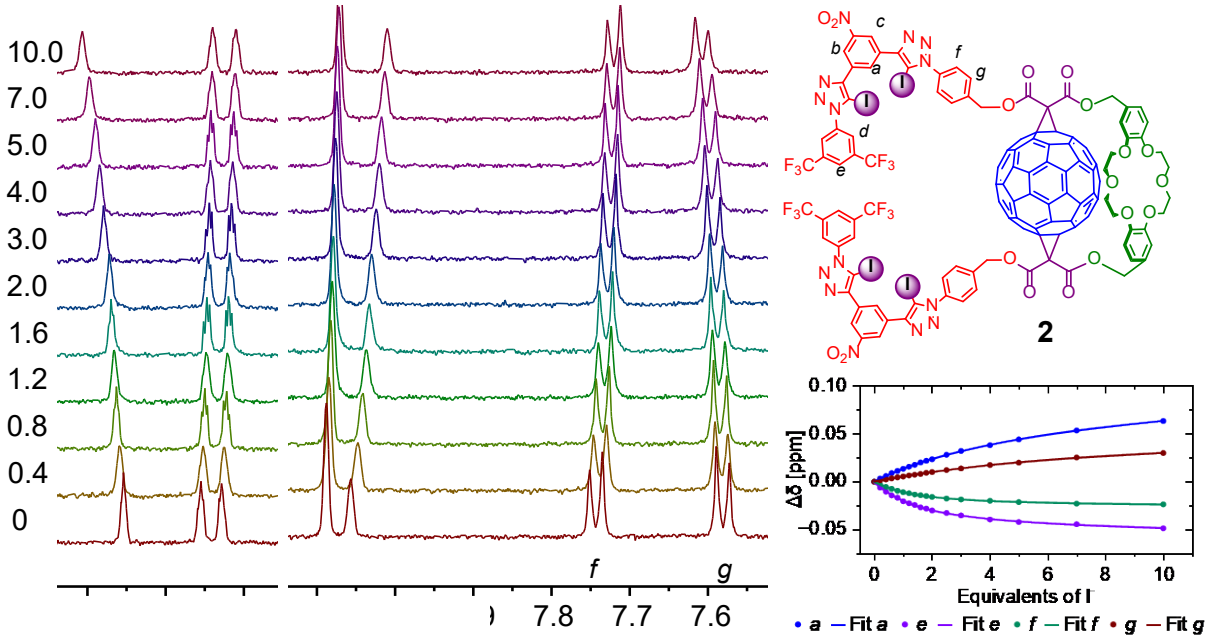

Figure 5. Truncated ^{1}H NMR spectra of receptor **2** in 3:1 $CDCl_3$:CD_3CN with increasing amount of TBAI. Corresponding binding isotherms used for determining values of binding constant.

Table 1. Halide anion association constants (K_a M^{-1}) for receptors 1, 2 and 16.

Anion		**1**[a]	**2**[a]	16[a]
Cl^-	$K_{1:1}$	3,600	2,400	2,700
	$K_{1:2}$	150	200	140
Br^-	$K_{1:1}$	5,200	2,900	4,000
	$K_{1:2}$	190	160	170
I^-	$K_{1:1}$	4,600	3,400	3,200
	$K_{1:2}$	180	140	160
[a]Solvent: 3:1 $CDCl_3$:CD_3CN at 298 K. Errors < 15%				

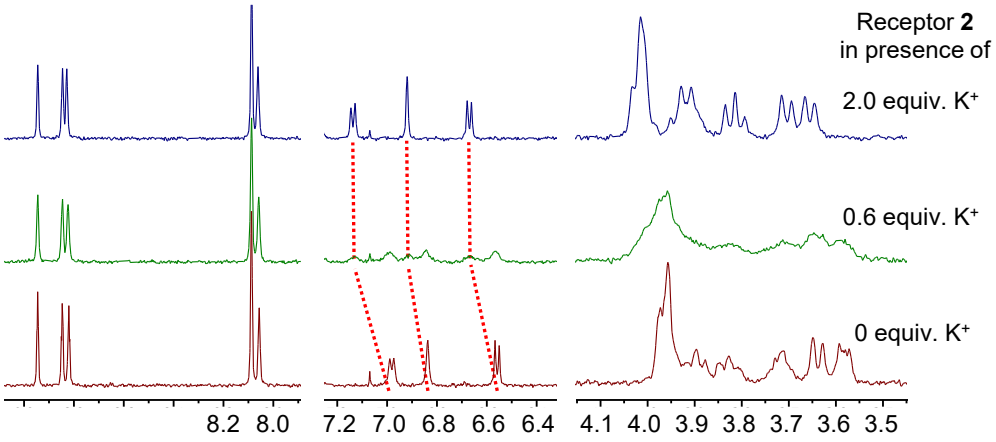

Figure 6. Truncated ^{1}H NMR spectra of receptor **2** in 3:1 $CDCl_3$:CD_3CN with increasing amount of $KBAr_4^F$.

conformational freedom to facilitate the formation of stronger XB-halide anion interactions in the 1:1 complex. Control receptor **16**, which does not contain fullerene, exhibits a halide selectivity trend mirroring that of **1**, however with lower $K_{1:1}$ values. Interestingly, receptor **2** exhibits a unique preference for I^- over Br^- and Cl^- which might be a result of a shorter distance between the XB binding units and the fullerene surface. The combination of the C_{60} fullerene scaffold's preorganization of the two XB anion binding arms proximal to the hydrophobic fullerene surface and possible additional anion-π interactions are most likely responsible for the enhanced binding of **1** and a unique iodide binding selectivity of **2**.

The cation binding properties of the fullerene containing receptors **1** and **2** were also investigated by ^{1}H NMR titration experiments in 3:1 $CDCl_3$:CD_3CN. Addition of $KBAr_4^F$ to solutions of free receptors **1** or **2** resulted in significant perturbations of the crown ether cation binding domain chemical shifts. With first aliquots of $KBAr_4^F$, notable signal broadening was observed, and a new set of signals emerged due to slow exchange on the NMR time scale (Figure 6). In particular, the aromatic proton signals of the receptor's DB18C6 motif experienced notable downfield shifts ($\Delta\delta \approx 0.10$ ppm), concomitant with -OCH_2- crown ether perturbations. After 1.4 equiv. of K^+ however, no further changes were observed, which is indicative of strong binding in a 1:1 stoichiometric host-guest complex. Importantly, no significant changes ($\Delta\delta < 0.01$ ppm) were observed in the proton signals of the XB anion binding domains of both receptors. This observation further corroborates a good separation of the anion binding domain from the cation one.

To investigate the ion-pair binding properties of receptors **1** and **2**, halide anion ^{1}H NMR titration experiments in the presence of one equivalent of $KBAr_4^F$ were undertaken. Addition of TBAI to a solution of K^+ complexed **1** or **2** caused perturbations of the XB anions binding sites, confirming that XB donors are involved in anion binding. In fact, these shift patterns were qualitatively similar to those observed during titrations of the free receptors. However, small changes were also observed in the -OCH_2- proton signals of the crown ether cation binding domains. Notably, the downfield perturbations of the -OCH_2- crown ether signals around 3.90 ppm were larger during titrations with bromide, and even greater with chloride (Figure 7). This perturbation pattern cannot be explained by simple potassium cation decomplexation of the crown ether and precipitation of the potassium halide salt (compare with spectra shown in Figure 6).

The aforementioned observations suggest the crown ether bound K^+ is directly involved in complexation of the anions. Interestingly, a qualitatively similar perturbation pattern of the crown ether signals was also observed during analogous titrations of K^+ complexed C_{60}-DB18C6 adduct **9**, which does not contain a XB anion binding domain (Figure 7). In this case, however, the overall signal shifts were more pronounced. In the presence of 1 equiv. of $KBAr_4^F$ receptor **9** forms 1:1 stoichiometric halide complexes with the preference for hard small anions: Cl^- > Br^- > I^- in 3:1 $CDCl_3$:CD_3CN, as determined by Bindfit analysis of binding isotherms (Table 2). This assembly is driven predominantly by electrostatic interactions with the crown ether complexed potassium cation resulting in the formation of a close contact ion-pair.

We suspect that such a binding mode is also present during titrations of receptors **1** and **2** with halides, particularly harder ones such as Cl^- and Br^-. However, due to spatial separation of the cation and anion binding domains in receptors **1** and **2**, two distinct types of 1:1 stoichiometric complex **A** and **B** can be simultaneously formed, contributing to the experimentally determined overall 1:1 association constants (Figure 8). In binding mode **A**, the anion is exclusively bound by the XB binding site, while in mode **B** the anion associates solely with the crown-ether bound potassium cation in a contact ion-pair recognition fashion.[61,62] Similarly, upon excess addition of anion, two types of 1:2 stoichiometric complexes are possible: **C** with two anions bound individually by the XB donor arms and **D**, in which one anion is bound in a tetradentate XB fashion and the other anion is associating with the potassium cation (Figure 8).

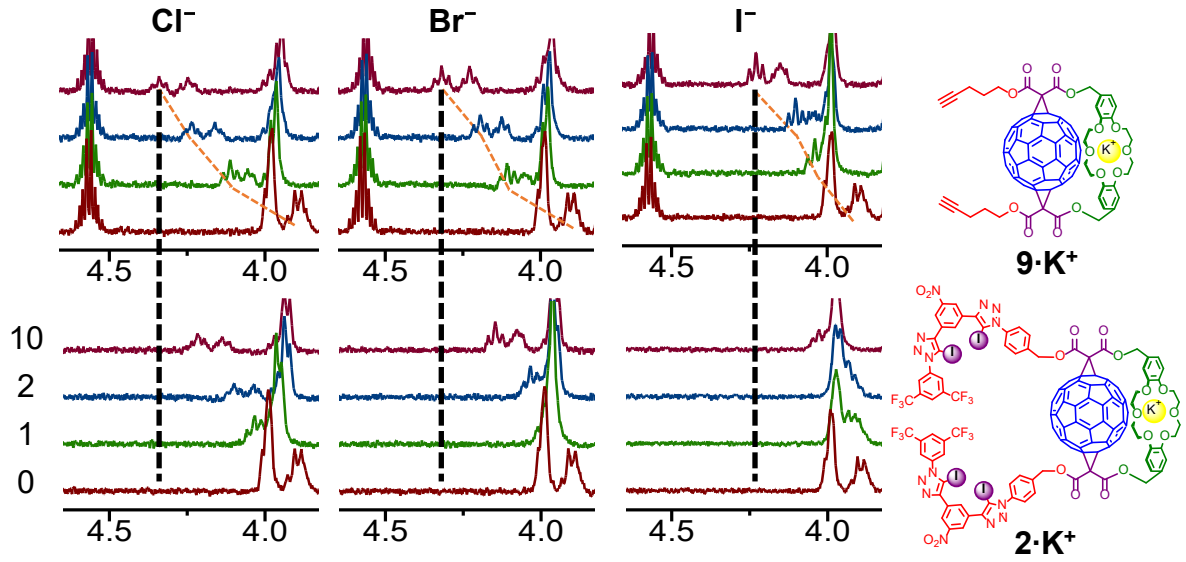

Figure 7. Comparison of crown ether regions during ^{1}H NMR titrations of receptors **9** (top) and **2** (bottom) in presence of 1 equiv. K^+ with TBA salts of Cl^-, Br^-, and I^-.

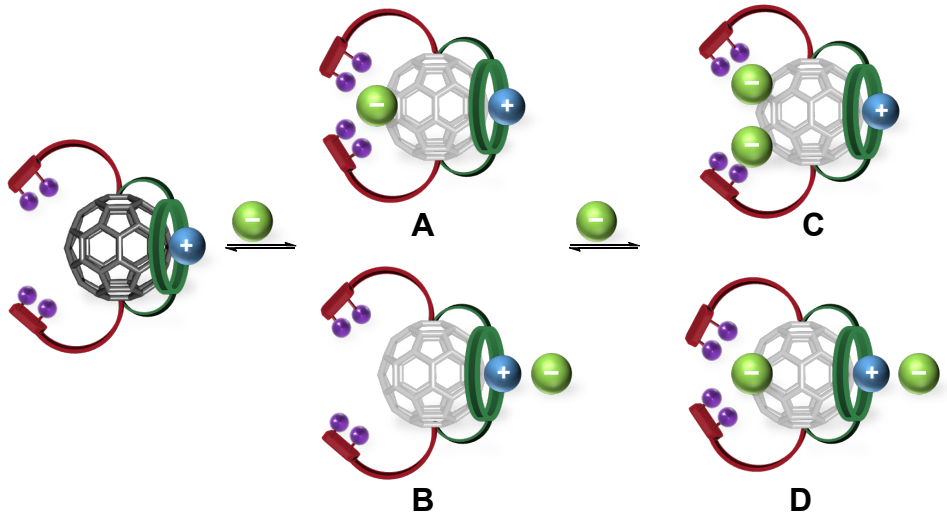

Figure 8. Proposed anion binding modes of fullerene functionalized halogen bonding heteroditopic hosts in presence of crown ether bound potassium cation.

This hypothesis was further corroborated by the ^{1}H NMR titration of **2**·K^+ with NO_3^-, which exhibits strong preference for the close contact ion-pair formation (mode **B**). During the titration with $TBANO_3$ no changes were observed in the XB anion binding domain, while significant perturbation of the crown ether signals was observed until ca. 1.5 equiv. of anion was added (Fig. S2.14). Addition of up to 10 equiv. NO_3^- had no further impact on the proton signals of **2**·K^+, suggesting the oxoanion forms only the 1:1 stoichiometric anion complex of mode **B**. Interestingly, addition of 2 equiv. of TBACl at the end of the titration with NO_3^- (10 equiv.) induced perturbations of XB binding domain signals and no changes of crown ether signals were observed. This confirms the independence of the anion binding sites and formation of type **D** complex with chloride occupying the XB binding domain and nitrate forming the contact ion-pair with the crown ether bound K^+.

Quantitative analysis of the halide binding isotherms in the presence of 1 equiv. of $KBAr_4^F$, using a 1:2 stoichiometric host-guest model, gave overall association constant values shown in Table 2, where $K_{1:1}$ represents the summation of 1:1 stoichiometric anion binding modes **A** & **B** and $K_{1:2}$ the 1:2 stoichiometric anion binding modes **C** & **D**. Comparing Table 1 and Table 2, the presence of the complexed K^+ in the respective C_{60}-DB18C6 cation binding domain of the XB receptors **1** and **2**, results in a significant enhancement of halide association constants, particularly of $K_{1:1}$. Importantly, it was possible to deconvolute and estimate the individual contributions of **A** & **B** halide binding modes to the overall $K_{1:1}$ association constant value through the analysis of the

chemical shifts of the crown ether protons of receptors **1** and **2**, and control receptor **9** during halide anion titrations in presence of $KBAr_4^F$ (see ESI for details). In the case of **1**, the binding mode **A** accounts for approximately 63% of the overall 1:1 chloride association constant, 83% of 1:1 bromide association constant, and more than 95% of 1:1 iodide association constant, clearly showing the preference of the heavier softer halide anions towards fullerene assisted XB binding. Further corroborating these estimates, the values of 1:1 association constants for mode **B** of receptors **1** and **2**, obtained using this method, are in good agreement with the values obtained during titrations of control receptor **9**, which is only able to bind anions via mode **B**.

Deconvolution of the **A** & **B** binding modes of 1:1 association enabled a direct comparison of K^+ coordination effects on the fullerene assisted halide binding in the XB domain. The $K_{1:1}$ association constant values for anion binding mode **A** ($K_{1:1}^A$) of both heteroditopic receptors **1** and **2** are significantly increased in the presence of co-bound K^+ (Table 3). Notably, the binding enhancement for I^- is particularly strong, resulting in a remarkably increased selectivity for iodide. In the case of receptor **2**, $K_{1:1}^A$ association constants increased by a factor $\alpha = 2.2$ ($\alpha = K_{1:1}^A(K^+)/K_{1:1}$) and 2.1 for chloride and bromide, respectively, while for iodide $\alpha = 5.2$. Even stronger I^- enhancement was observed for receptor **1** ($\alpha = 7.4$), however overall selectivity of **1** for I^- *vs.* other halides is reduced in comparison with **2**. In the presence of co-bound K^+, control heteroditopic receptor **16**, without the fullerene scaffold, binds all the halides significantly more strongly (α = 12.7 – 13.5), however notably at the expense of much lower selectivity. This is most likely due to the formation of a close contact ion pair resulting in stronger electrostatic interactions. The remarkable properties and influence of C_{60} for ion recognition is particularly evident in comparison of iodide binding affinity exhibited by **1** and **16**. Impressively, the iodide $K_{1:1}$ association constant value of receptor **1**, whose anion and cation binding domains are separated by the fullerene, almost matches the magnitude for receptor **16**, which is capable of anion binding assisted by close contact with the crown ether co-bound potassium cation. Importantly, this suggests that the polarizing C_{60} surface can elicit particularly strong interactions with polarizable soft anion species such as iodide and transfer electrostatic effects over significant distances within the fullerene heteroditopic host design.

Table 2. Overall anion association constants ($K_{1:1}$, $K_{1:2}$ /M^{-1}) for receptors 1, 2, 9 in presence of 1 equiv. K^+.

Anion		**1**[a]	**2**[a]	**9**[a]
Cl^-	$K_{1:1}$	15,100	9,300	5,000
	$K_{1:2}$	490	400	-[b]
Br^-	$K_{1:1}$	25,600	8,400	2,700
	$K_{1:2}$	330	280	-[b]
I^-	$K_{1:1}$	36,000	19,800	1,400
	$K_{1:2}$	600	610	-[b]

[a]Solvent: 3:1 $CDCl_3$:CD_3CN at 298 K. Errors < 15%. [b]Not formed.

Table 3. Anion association constants for receptors 1, 2 ($K_{1:1}^A$, M^{-1}, anion binding mode A) and 16 ($K_{1:1}$, M^{-1}) in presence of 1 equiv. K^+.

	1			**2**			**16**	
Anion	$K_{1:1}^A$[a]	α[b]	**A**[c]	$K_{1:1}^A$[a]	α[b]	**A**[c]	$K_{1:1}$[a]	α[b]
Cl^-	9,500	2.6	63%	5,300	2.2	57%	34,200	12.7
Br^-	21,200	4.1	83%	6,100	2.1	73%	54,000	13.5
I^-	34,200	7.4	>95%	17,800	5.2	>90%	43,100	13.5

[a]Solvent: 3:1 $CDCl_3$:CD_3CN at 298 K. Errors < 15%. [b]Binding enhancement factors in presence of K^+; [c]Contributions of anion binding mode **A** to overall 1:1 binding

Computational analysis. Having demonstrated the unique ion-pair recognition properties of fullerene-containing heteroditopic receptors **1** and **2**, DFT calculations were undertaken to gain insight into the electronic and structural aspects of the ion-pair complexation. In the computational analysis, we focused on receptor **2**, which manifested the highest selectivity, presumably due to the closer proximity of the fullerene surface. DFT calculations in the gas-phase were carried out with Gaussian16,[63] using the M06-2X functional, chosen for its ability to accurately describe halogen bonds and π-π stacking interactions.[64–66] The Def2-SVP basis set was selected,[67] except for the anions and iodine binding units, which were described with the Def2-TZVPD basis set,[67,68] taken from the Basis Set Exchange website.[69–71] This combination was employed to balance the accurate description of the non-covalent interactions and the structural features of the large receptors **1** and **2**.

The MEP surface of C_{60} (Figure 1) exhibits distinct electrophilic regions, with π-holes situated above its twelve five-membered (C_5) rings and twenty six-membered (C_6) rings. These π-holes have molecular surface electrostatic potential (V_S) values ranging between 7.2 and 7.9 kcal mol^{-1}. For comparison, **9** and its K^+ complex were also optimized by DFT (Figure 9). The DB18C6 motif in adduct **9** has a significant impact on the electrostatic potential map, resulting in a nearly negatively charged fullerene surface. The exposed surface of the fullerene displays several π-holes with V_S values ranging between -5.5 and -0.2 kcal mol^{-1}. The lowest V_S values of **9** were found between the oxygen atoms of the crown-ether cavity, varying between -58.6 and -57.5 kcal mol^{-1}. The MEP surface of **9**'s C_{60} moiety has an additional negative point of V_S with -29.5 kcal mol^{-1}, perpendicular to the C_6 ring just below the crown ether. This electron rich site is perfectly prepared for coordination of K^+, as evidenced by a computed $K^+\cdots C_6$ distance of 2.93 Å in **9**·K^+. The potassium cation binding induces significant redistribution of the electrostatic potential in **9**, with the C_{60} π-holes' V_S values now ranging from 30.4 to 47.2 kcal mol^{-1}. For comparison, typical π-hole donors trifluoro-1,3,5-triazene or hexafluorobenzene,[72] investigated at the M06-2X/Def2-SVP theory level, respectively display $V_{s,max}$ values of 40.9 and 21.5 kcal mol^{-1}. However, in complex **9**·K^+, the $V_{S,max}$ of 111.8 kcal mol^{-1} is found over the metal cation, which explains its strong tendency to form close putative ion-pair contacts with halides, as depicted in Figure S5.1 with the DFT optimized structures of **9**·K·X (X = Cl, Br, or I) complexes. The computed $K^+\cdots X^-$ distances (Cl^-: 2.85; Br^-: 3.02; and I^-: 3.23 Å) mirror the anion's size, with the shortest contact corresponding to the highest association constant, found for **9**·KCl (Table 2).

The starting geometries of **1** and **2** were generated *via* crude gas-phase MD simulations of KCl complexes, enforcing halogen bonds through geometric restraints, as detailed in the ESI. Multiple conformations were selected and subsequently subjected to geometry optimizations using DFT. Figure 10 shows the optimized structures of chloride complexes of **2** with potassium hosted within the DB18C6 cation binding domain for the **A**-**D** anion binding scenarios, consistent with the binding modes hypothesized based on ^{1}H NMR titrations, while Figures S5.2 and S5.3 show equivalent optimized binding arrangements for bromide and iodide.

Potassium binding by the DB18C6 moiety can be characterized by $K^+\cdots C_6$ distances summarized in Table S5.1. In scenarios **A** and **C**, the average $K^+\cdots C_6$ distance is *ca*. 3 Å and

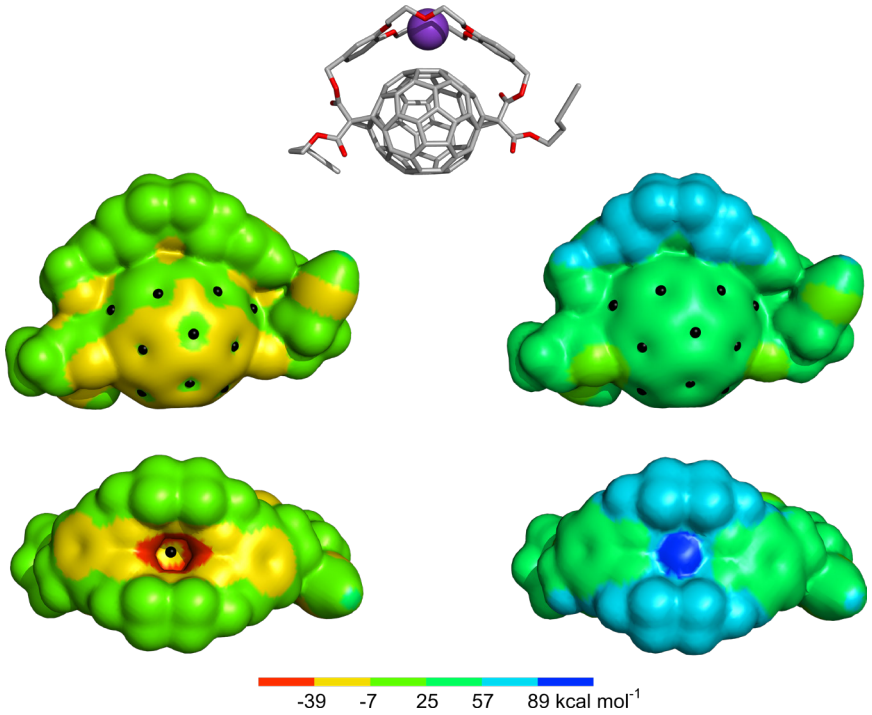

Figure 9. DFT optimized structure of **9**·K^+ (centre, top), together with the MEP surfaces calculated on the adduct free of potassium (left) or on the complex (right), in lateral and top views. The π-holes on the surface of the C_{60} scaffold are identified with black dots.

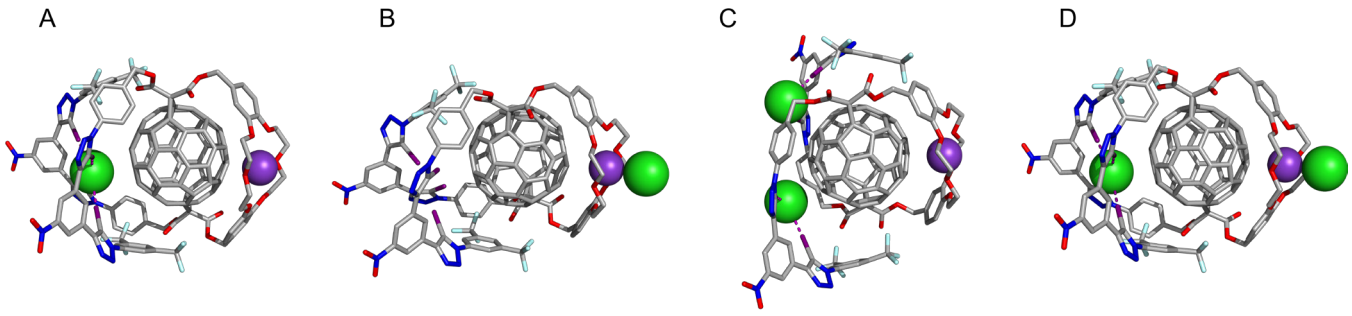

Figure 10. DFT optimized anion binding modes of fullerene functionalized halogen bonding heteroditopic host **2** in presence of the crown ether complexed potassium cation.

is independent of the halide present in the anion binding domain. In binding mode **B** the values of the $K^+\cdots C_6$ distances are significantly larger, ranging between 3.53 and 3.79 Å and depend on the complexed halide. Due to the close ion-pair contact, the anion pulls K^+ from the crown ether, weakening the potential interaction with the fullerene surface.[54] Interestingly, in scenario **D**, the $K^+\cdots C_6$ distances have intermediate values between those computed for **B** and **A**/**C**, showing that binding in one domain can influence the behavior on the opposite side.

In binding mode **A**, the four convergent halogen bonds with chloride are not equivalent (Table S5.2). Two interactions have an average $I\cdots Cl^-$ distance of 3.35 Å and an average C-I$\cdots Cl^-$ angle of 163°, while the other two interactions are nearly linear with distances of 3.03 Å and angles of 173°, consistent with highly localized σ-hole XB interactions. The XB distances and angles in the bromide (3.58 Å, 162°; 3.21 Å, 174°) and iodide (3.83 Å, 162°; 3.43 Å, 176°) complexes follow a similar pattern, adjusted for the sizes of the ions (Table S5.2). This asymmetry is not surprising considering the differences in the iodo-triazole units of the anion binding domain. One is directly connected to a strong electron withdrawing 3,5-bis(trifluoromethyl)phenyl group, while the other is connected to an electron-rich alkyl-substituted phenyl. Importantly, the halogen bonding anions' recognition is assisted by anion-π interactions with short contacts between the fullerene surface and each anion, leading to the trend of $C_6\cdots X^-$ distances Cl^- (3.15 Å) < Br^- (3.36 Å) < I^- (3.64 Å).

After establishing the putative binding arrangements for the recognition of halides in binding modes **A**-**D**, the MEP maps of **2** and **2**·K^+ were evaluated through single-point DFT calculations. To achieve this, we used the optimized structure of the Cl^- association in scenario **D** and removed the necessary ions (Figure 11). The most negative region of electrostatic potential on the electronic surface of **2** covers the oxygen atoms of the crown-ether (including the $V_{S,min}$ of -45.8 kcal mol^{-1}), whilst the most positive regions are found in front of the iodine binding clefts, with their σ-holes characterized by V_S values of 43.6 and 44.3 kcal mol^{-1}, and of 48.2 and 48.3 kcal mol^{-1} for the iodo-triazole unit activated by neighboring -CF_3 groups. Complexation of K^+ in the cation binding domain of **2** leads to a significant redistribution of the MEP surface. Naturally, the $V_{S,max}$ of 130.2 kcal mol^{-1} is located over the cation, however the four XB units display augmented V_S values between 75.3 and 79.7 kcal mol^{-1}. Notably, a V_S point of 61.5 kcal mol^{-1} was found positioned over the C_6 ring in the vicinity of the preorganized XB binding units.

The strength of the XB interactions in different binding modes was further evaluated with the Natural Bond Orbital (NBO) analysis, using the Second Order perturbation theory interaction energies (E^2, see Table S5.3). The analysis of the E^2 values for the interactions between the C–I antibonding orbitals of **2** and the halides' lone pairs orbitals ($n_X \rightarrow \sigma^*_{C\text{-}I}$) revealed that in binding mode **A** the total energies follow the trend: Cl^- (37.5 kcal mol^{-1}) > Br^- (36.3 kcal mol^{-1}) > I^- (33.1 kcal mol^{-1}). A similar analysis was also performed for the interactions between the fullerene scaffold's π-holes and the three halides, revealing that E^2 values resulting from $n_X \rightarrow \sigma^*_{C\text{-}C}$ are over an order of magnitude weaker (0.5-1.3 kcal mol^{-1}) than the XB interactions.

Although the computational analysis suggests that in the gas phase binding mode **B** is preferred for **2** by 3.0 (Cl^-), 5.1 (Br^-), and 6.2 (I^-) kcal mol^{-1}, it is worth noting that in the case of **1**·KCl, binding mode **A** is favored by 24.9 kcal mol^{-1} relatively to **B** (Figure S5.4).[73] In this complex, however, the halide does not form a contact with the fullerene surface and the receptor adopts a conformation which maximizes the strength of the halogen bonding.

Altogether, the computational analysis reveals that the fullerene platform can play a dual role in the anion binding by receptors **1** and **2**. Indeed, it can be actively involved in

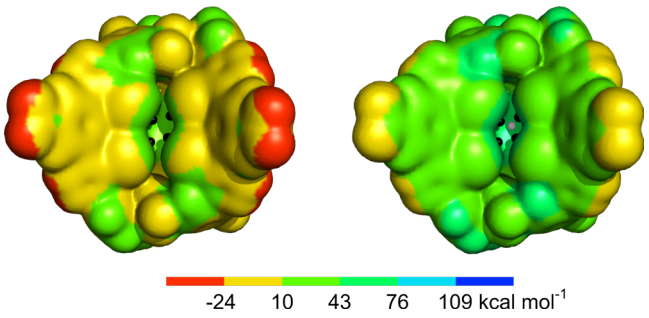

Figure 11. MEP surfaces calculated on the DFT optimized geometry of **2** in binding scenario **D** (Figure 10D): free of ions (left) and in the presence of K^+ (right). The σ-holes in front of the XB binding units are identified with black dots, while a neighbouring π-hole on the surface of the C_{60} scaffold is identified with a white dot.

the binding events by exploiting π-holes on its surface, but it can also serve as a bulky scaffold to preorganize the potent XB-based binding units into a tight binding cavity.

Conclusions

For the first time, the C_{60} fullerene motif has been successfully integrated into a heteroditopic ion-pair host design. The combination of highly potent XB donors and a crown ether moiety separated by C_{60} led to rationally designed receptors with ion-pair binding properties influenced and modulated by the fullerene motif. Receptors **1** and **2**, which differ in length of linkers separating anion binding motifs from the fullerene surface, are capable of strong and more selective binding of halide anions than their non-fullerene analogue. This is achieved by preorganization of binding units, solvent shielding, and π-hole assistance provided by the bulky and highly polarizable C_{60} architecture. Remarkable halide anion binding enhancements can be achieved by the complexation of a potassium cation by the rigid crown ether moiety located close to the fullerene surface. Notably, potassium binding by receptors **1** and **2** results in strong augmented iodide binding selectivity, with association constants matching the value of the non-fullerene heteroditopic receptor analogue which is capable of anion binding assisted by the close contact with the crown ether co-bound potassium cation.

Fullerene spatial separation of XB donors and the crown ether complexed K^+ resulted in a rare example of an artificial receptor containing two anion binding sites with opposing preferences for hard and soft halides. Detailed analysis of ^{1}H NMR titration data allowed for deconvolution of the ion-pair binding modes contributing to the overall 1:1 stoichiometric halide anion binding by **1**·K^+ and **2**·K^+. Soft polarizable iodide was bound almost exclusively (> 90%) by the tetradentate XB binding domain in proximity to the fullerene surface. This binding mode also dominated in the case of smaller and harder chloride (ca. 60%), however, a significant portion of chloride (ca. 40%) was associated in a close contact ion-pair with the crown ether bound potassium cation without assistance of the XB binding domains.

Altogether, the presented results demonstrate the unprecedented potential of fullerene surfaces in anion recognition host-guest chemistry. Importantly, polarizing the C_{60} surface *via* proximal cation recognition can elicit particularly strong interactions with polarizable soft anion species such as iodide and transfer electrostatic effects over significant distances. Modulating the properties of fullerene-based compounds *via* reversible non-covalent charged guest recognition has exciting future potential applications in molecular sensors, solar cell devices, and photodynamic therapy.

ASSOCIATED CONTENT

Supporting Information is available.
Experimental procedures and methods, NMR spectra, titration data, additional data, and figures

Accession Codes
CCDC 2282543 contain the supplementary crystallographic data for this paper. These data can be obtained free of charge via www.ccdc.cam.ac.uk/data_request/cif, or by emailing data_request@ccdc.cam.ac.uk, or by contacting The Cambridge Crystallographic Data Centre, 12 Union Road, Cambridge CB2 1EZ, UK; fax: +44 1223 336033.

AUTHOR INFORMATION

Corresponding Author

Paul D. Beer – Chemistry Research Laboratory, Department of Chemistry, University of Oxford, Oxford OX1 3TA, U.K.; orcid.org/0000-0003-0810-9716; email: paul.beer@chem.ox.ac.uk
Vítor Félix – *CICECO - Aveiro Institute of Materials, Department of Chemistry, University of Aveiro, 3810-193 Aveiro, Portugal*; orcid.org/0000-0001-9380-0418; email: vitor.felix@ua.pt

Authors

Krzysztof M. Bąk – Chemistry Research Laboratory, Department of Chemistry, University of Oxford, Oxford OX1 3TA, U.K.; orcid.org/0000-0003-4813-4887
Igor Marques – CICECO- Aveiro Institute of Materials, Department of Chemistry, University of Aveiro, 3810-193 Aveiro, Portugal; orcid.org/0000-0003-4971-9932
Heike Kuhn – Chemistry Research Laboratory, Department of Chemistry, University of Oxford, Oxford OX1 3TA, U.K.;
Kirsten E. Christensen – Chemistry Research Laboratory, Department of Chemistry, University of Oxford, Oxford OX1 3TA, U.K.;

Present Addresses

†**Krzysztof M. Bąk** – School of Chemistry, University of Edinburgh, Edinburgh, U.K.

Author Contributions

All authors have given approval to the final version of the manuscript.

ACKNOWLEDGMENT

KMB acknowledges EPSRC for postdoctoral funding (EPSRC grant number EP/P033490/1). The theoretical studies were developed within the scope of the project CICECO-Aveiro Institute of Materials, UIDB/50011/2020, UIDP/50011/2020 & LA/P/0006/2020, financed by national funds through the FCT/MCTES (PIDDAC). We would also like to thank Diamond Light Source for an award of beamtime (CY26802).

REFERENCES

(1) *Supramolecular Chemistry of Fullerenes and Carbon Nanotubes:* Martín, N., Nierengarten, J.-F., Eds.; Wiley-VCH Verlag GmbH & Co. KGaA, 2012.
(2) *Fullerenes: Chemistry and Reactions*, Hirsch, A.; Bretreich, M., Eds.; Wiley, 2004.
(3) Hirao, T.; Haino, T. Supramolecular Ensembles Formed via Calix[5]Arene-Fullerene Host-Guest Interactions. *Chem. Asian J.* **2022**, *17*, e202200344.
(4) Pérez, E. M.; Martín, N. Curves Ahead: Molecular Receptors for Fullerenes Based on Concave–Convex Complementarity. *Chem. Soc. Rev.* **2008**, *37*, 1512–1519.

(5) Yamada, M. Unraveling the Nature and Strength of Non-Covalent Interactions on the Surface of Fullerenes. *ChemPlusChem* **2023**, *88*, e202300062.

(6) Yamada, M.; Narita, H.; Maeda, Y. A Fullerene-Based Molecular Torsion Balance for Investigating Noncovalent Interactions at the C $_{60}$ Surface. *Angew. Chem. Int. Ed.* **2020**, *59*, 16133–16140.

(7) Lu, Z.; Ronson, T. K.; Heard, A. W.; Feldmann, S.; Vanthuyne, N.; Martinez, A.; Nitschke, J. R. Enantioselective Fullerene Functionalization through Stereochemical Information Transfer from a Self-Assembled Cage. *Nat. Chem.* **2023**, *15*, 405–412.

(8) Chen, Q.; Thompson, A. L.; Christensen, K. E.; Horton, P. N.; Coles, S. J.; Anderson, H. L. β,β-Directly Linked Porphyrin Rings: Synthesis, Photophysical Properties, and Fullerene Binding. *J. Am. Chem. Soc.* **2023**, *145*, 11859–11865.

(9) Moreno-Simoni, M.; Torres, T.; De La Torre, G. Subphthalocyanine Capsules: Molecular Reactors for Photoredox Transformations of Fullerenes. *Chem. Sci.* **2022**, *13*, 9249–9255.

(10) Hasegawa, S.; Meichsner, S. L.; Holstein, J. J.; Baksi, A.; Kasanmascheff, M.; Clever, G. H. Long-Lived C_{60} Radical Anion Stabilized Inside an Electron-Deficient Coordination Cage. *J. Am. Chem. Soc.* **2021**, *143*, 9718–9723.

(11) Rothschild, D. A.; Kopcha, W. P.; Tran, A.; Zhang, J.; Lipke, M. C. Gram-Scale Synthesis of a Covalent Nanocage That Preserves the Redox Properties of Encapsulated Fullerenes. *Chem. Sci.* **2022**, *13*, 5325–5332.

(12) Barendt, T. A.; Myers, W. K.; Cornes, S. P.; Lebedeva, M. A.; Porfyrakis, K.; Marques, I.; Félix, V.; Beer, P. D. The Green Box: An Electronically Versatile Perylene Diimide Macrocyclic Host for Fullerenes. *J. Am. Chem. Soc.* **2020**, *142*, 349–364.

(13) Fuertes-Espinosa, C.; García-Simón, C.; Pujals, M.; Garcia-Borràs, M.; Gómez, L.; Parella, T.; Juanhuix, J.; Imaz, I.; Maspoch, D.; Costas, M.; Ribas, X. Supramolecular Fullerene Sponges as Catalytic Masks for Regioselective Functionalization of C60. *Chem* **2020**, *6*, 169–186.

(14) Megiatto, J. D.; Guldi, D. M.; Schuster, D. I. Design, Synthesis and Photoinduced Processes in Molecular Interlocked Photosynthetic [60]Fullerene Systems. *Chem. Soc. Rev.* **2020**, *49*, 8–20.

(15) Pan, Y.; Liu, X.; Zhang, W.; Liu, Z.; Zeng, G.; Shao, B.; Liang, Q.; He, Q.; Yuan, X.; Huang, D.; Chen, M. Advances in Photocatalysis Based on Fullerene C60 and Its Derivatives: Properties, Mechanism, Synthesis, and Applications. *Appl. Catal. B* **2020**, *265*, 118579.

(16) Guldi, D. M.; Illescas, B. M.; Atienza, C. M.; Wielopolski, M.; Martín, N. Fullerene for Organic Electronics. *Chem. Soc. Rev.* **2009**, *38*, 1587–1597.

(17) Lee, C.; Seo, Y.; Han, J.; Hwang, J.; Jeon, I. Perspectives on Critical Properties of Fullerene Derivatives for Rechargeable Battery Applications. *Carbon* **2023**, *210*, 118041.

(18) Collavini, S.; Delgado, J. L. Fullerenes: The Stars of Photovoltaics. *Sustain. Energy Fuels* **2018**, *2*, 2480–2493.

(19) Gatti, T.; Menna, E.; Meneghetti, M.; Maggini, M.; Petrozza, A.; Lamberti, F. The Renaissance of Fullerenes with Perovskite Solar Cells. *Nano Energy* **2017**, *41*, 84–100.

(20) Castro, E.; Garcia, A. H.; Zavala, G.; Echegoyen, L. Fullerenes in Biology and Medicine. *J. Mater. Chem. B* **2017**, *5*, 6523–6535.

(21) Lebedeva, M. A.; Chamberlain, T. W.; Khlobystov, A. N. Harnessing the Synergistic and Complementary Properties of Fullerene and Transition-Metal Compounds for Nanomaterial Applications. *Chem. Rev.* **2015**, *115*, 11301–11351.

(22) Babu, S. S.; Möhwald, H.; Nakanishi, T. Recent Progress in Morphology Control of Supramolecular Fullerene Assemblies and Its Applications. *Chem. Soc. Rev.* **2010**, *39*, 4021–4035.

(23) Martín, N.; Sánchez, L.; Herranz, M. Á.; Illescas, B.; Guldi, D. M. Electronic Communication in Tetrathiafulvalene (TTF)/C_{60} Systems: Toward Molecular Solar Energy Conversion Materials? *Acc. Chem. Res.* **2007**, *40*, 1015–1024.

(24) Chen, D.; Liu, S.; Chen, D.; Liu, J.; Wu, J.; Wang, H.; Su, Y.; Kwak, G.; Zuo, X.; Rao, D.; Cui, H.; Shu, C.; Suk, J. S. A Two-Pronged Pulmonary Gene Delivery Strategy: A Surface-Modified Fullerene Nanoparticle and a Hypotonic Vehicle. *Angew. Chem. Int. Ed.* **2021**, *60*, 15225–15229.

(25) Izquierdo, M.; Platzer, B.; Stasyuk, A. J.; Stasyuk, O. A.; Voityuk, A. A.; Cuesta, S.; Solà, M.; Guldi, D. M.; Martín, N. All-Fullerene Electron Donor–Acceptor Conjugates. *Angew. Chem. Int. Ed.* **2019**, *58*, 6932–6937.

(26) Barendt, T. A.; Rašović, I.; Lebedeva, M. A.; Farrow, G. A.; Auty, A.; Chekulaev, D.; Sazanovich, I. V.; Weinstein, J. A.; Porfyrakis, K.; Beer, P. D. Anion-Mediated Photophysical Behavior in a C_{60} Fullerene [3]Rotaxane Shuttle. *J. Am. Chem. Soc.* **2018**, *140*, 1924–1936.

(27) Zhang, Y.; Wang, D.; Wang, W. Beyond the σ-Hole and π-Hole: The Origin of the Very Large Electrophilic Regions of Fullerenes and Carbon Nanotubes. *Comput. Theor. Chem.* **2018**, *1128*, 56–59.

(28) López-Andarias, J.; Bauzá, A.; Sakai, N.; Frontera, A.; Matile, S. Remote Control of Anion-π Catalysis on Fullerene-Centered Catalytic Triads. *Angew. Chem. Int. Ed.* **2018**, *57*, 10883–10887.

(29) Zhang, X.; Liu, L.; López-Andarias, J.; Wang, C.; Sakai, N.; Matile, S. Anion-π Catalysis: Focus on Nonadjacent Stereocenters. *Helv. Chim. Acta* **2018**, *101*, e1700288.

(30) López-Andarias, J.; Frontera, A.; Matile, S. Anion–π Catalysis on Fullerenes. *J. Am. Chem. Soc.* **2017**, *139*, 13296–13299.

(31) Sun, X.; Chen, W.; Liang, L.; Hu, W.; Wang, H.; Pang, Z.; Ye, Y.; Hu, X.; Wang, Q.; Kong, X.; Jin, Y.; Lei, M. Construction of Electron Transfer Network by Self-Assembly of Self-n-Doped Fullerene Ammonium Iodide. *Chem. Mater.* **2016**, *28*, 8726–8731.

(32) Sun, S.; Liu, Z.; Colombo, F.; Gao, R.; Yu, Y.; Qiu, Y.; Su, J.; Gan, L. Open-Cage Fullerene as Molecular Container for F-, Cl- , Br- and I-. *Angew. Chem. Int. Ed.* **2022**, *61*, e202212090.

(33) Anstöter, C. S.; Rogers, J. P.; Verlet, J. R. R. Spectroscopic Determination of an Anion–π Bond Strength. *J. Am. Chem. Soc.* **2019**, *141*, 6132–6135.

(34) Kepler, S.; Zeller, M.; Rosokha, S. V. Anion–π Complexes of Halides with P-Benzoquinones: Structures, Thermodynamics, and Criteria of Charge Transfer to Electron Transfer Transition. *J. Am. Chem. Soc.* **2019**, *141*, 9338–9348.

(35) Molina, P.; Zapata, F.; Caballero, A. Anion Recognition Strategies Based on Combined Noncovalent Interactions. *Chem. Rev.* **2017**, *117*, 9907–9972.

(36) Giese, M.; Albrecht, M.; Rissanen, K. Anion–π Interactions with Fluoroarenes. *Chem. Rev.* **2015**, *115*, 8867–8895.

(37) Sabirov, D. Sh. Polarizability as a Landmark Property for Fullerene Chemistry and Materials Science. *RSC Adv.* **2014**, *4*, 44996–45028.

(38) Bąk, K. M.; Patrick, S. C.; Li, X.; Beer, P. D.; Davis, J. J. Engineered Binding Microenvironments in Halogen Bonding Polymers for Enhanced Anion Sensing. *Angew. Chem. Int. Ed.* **2023**, *62*, e202300867.

(39) Liu, Y.; Parks, F. C.; Sheetz, E. G.; Chen, C.-H.; Flood, A. H. Polarity-Tolerant Chloride Binding in Foldamer Capsules by Programmed Solvent-Exclusion. *J. Am. Chem. Soc.* **2021**, *143*, 3191–3204.

(40) Docker, A.; Marques, I.; Kuhn, H.; Zhang, Z.; Félix, V.; Beer, P. D. Selective Potassium Chloride Recognition, Sensing, Extraction, and Transport Using a Chalcogen-Bonding Heteroditopic Receptor. *J. Am. Chem. Soc.* **2022**, *144*, 14778–14789.

(41) Tay, H. M.; Tse, Y. C.; Docker, A.; Gateley, C.; Thompson, A. L.; Kuhn, H.; Zhang, Z.; Beer, P. D. Halogen-Bonding Heteroditopic [2]Catenanes for Recognition of Alkali Metal/Halide Ion Pairs. *Angew. Chem. Int. Ed.* **2023**, *62*, e202214785.

(42) Grauwels, G.; Valkenier, H.; Davis, A. P.; Jabin, I.; Bartik, K. Repositioning Chloride Transmembrane Transporters: Transport of Organic Ion Pairs. *Angew. Chem. Int. Ed.* **2019**, *58*, 6921–6925.

(43) Hale, U. A.; Madhavan, N. Hydrophobic Cyclic Dipeptides as M^+/Cl^- Carriers. *Chem. Commun.* **2023**, *59*, 7068–7071.

(44) Walczak, W.; Zakrzewski, M.; Cichowicz, G.; Piątek, P. Complexation of 5-Aminovaleric Acid Zwitterions in Aqueous/Methanol Solution by Heterotopic Tri-Cationic Receptors. *Org. Biomol. Chem.* **2020**, *18*, 694–699.

(45) Rubio, O. H.; Taouil, R.; Muñiz, F. M.; Monleón, L. M.; Simón, L.; Sanz, F.; Morán, J. R. A Molecular Receptor Selective for Zwitterionic Alanine. *Org. Biomol. Chem.* **2017**, *15*, 477–485.

(46) McConnell, A. J.; Docker, A.; Beer, P. D. From Heteroditopic to Multitopic Receptors for Ion-Pair Recognition: Advances in Receptor Design and Applications. *ChemPlusChem* **2020**, *85*, 1824–1841.

(47) McConnell, A. J.; Beer, P. D. Heteroditopic Receptors for Ion-Pair Recognition. *Angew. Chem. Int. Ed.* **2012**, *51*, 5052–5061.

(48) Kim, S. K.; Sessler, J. L. Ion Pair Receptors. *Chem. Soc. Rev.* **2010**, *39*, 3784–3809.

(49) Pancholi, J.; Beer, P. D. Halogen Bonding Motifs for Anion Recognition. *Coord. Chem. Rev.* **2020**, *416*, 213281.

(50) Lim, J. Y. C.; Beer, P. D. Sigma-Hole Interactions in Anion Recognition. *Chem* **2018**, *4*, 731–783.

(51) Brown, A.; Beer, P. D. Halogen Bonding Anion Recognition. *Chem. Commun.* **2016**, *52*, 8645–8658.

(52) Gilday, L. C.; Robinson, S. W.; Barendt, T. A.; Langton, M. J.; Mullaney, B. R.; Beer, P. D. Halogen Bonding in Supramolecular Chemistry. *Chem. Rev.* **2015**, *115*, 7118–7195.

(53) Meijer, M. D.; van Klink, G. P. M.; van Koten, G. Metal-Chelating Capacities Attached to Fullerenes. *Coord. Chem. Rev.* **2002**, *230*, 141–163.

(54) Bourgeois, J.-P.; Seiler, P.; Fibbioli, M.; Pretsch, E.; Diederich, F.; Echegoyen, L. Cyclophane-Type Fullerene-dibenzo[18]Crown-6 Conjugates with Trans-1, Trans-2, and Trans-3 Addition Patterns: Regioselective Templated Synthesis, X-Ray Crystal Structure, Ionophoric Properties, and Cation-Complexation-Dependent Redox Behavior. *Helv. Chim. Acta* **1999**, *82*, 1572–1595.

(55) Bourgeois, J.-P.; Echegoyen, L.; Fibbioli, M.; Pretsch, E.; Diederich, F. Regioselective Synthesis of Trans-1 Fullerene Bis-Adducts Directed by a Crown Ether Tether: Alkali Metal Cation Modulated Redox Properties of Fullerene–Crown Ether Conjugates. *Angew. Chem. Int. Ed.* **1998**, *37*, 2118–2121.

(56) Bickerton, L. E.; Docker, A.; Sterling, A. J.; Kuhn, H.; Duarte, F.; Beer, P. D.; Langton, M. J. Highly Active Halogen Bonding and Chalcogen Bonding Chloride Transporters with Non-Protonophoric Activity. *Chem. Eur. J.* **2021**, *27*, 11738–11745.

(57) Low temperature single crystal X-ray diffraction data were collected on Diamond Light Source, beamline I19-1. Raw frame data were reduced using XIA2 and the structures were solved using 'Superflip' (a) Palatinus, L.; Chapuis, G. SUPERFLIP - a Computer Program for the solution of Crystal Structures by Charge Flipping in Arbitrary Dimensions. *J. Appl. Cryst.* **2007**, *40*, 786-790. before refinement with CRYSTALS (b) Parois, P.; Cooper, R. I.; Thompson, A. L. Crystal Structures of Increasingly Large Molecules: Meeting the Challenges with CRYSTALS Software. *Chem. Cent. J.* **2015**, 9:30. (c) Cooper, R. I.; Thompson, A. L.; Watkin, D. J. J. CRYSTALS Enhancements: Dealing with Hydrogen Atoms in Refinement. *Appl. Cryst.* **2010**, *43*, 1100-1107. as per the SI (CIF).

(58) Iehl, J.; Osinska, I.; Louis, R.; Holler, M.; Nierengarten, J.-F. A Stable Fullerene-Azide Building Block for the Construction of a Fullerene–Porphyrin Conjugate. *Tetrahedron Lett.* **2009**, *50*, 2245–2248.

(59) Iehl, J.; de Freitas, R. P.; Nierengarten, J.-F. Click Chemistry with Fullerene Derivatives. *Tetrahedron Lett.* **2008**, *49*, 4063–4066.

(60) Pereira de Freitas, R.; Iehl, J.; Delavaux-Nicot, B.; Nierengarten, J.-F. Synthesis of Fullerene Building Blocks Bearing Alkyne or Azide Groups and Their Subsequent Functionalization by the Copper Mediated Huisgen 1,3-Dipolar Cycloaddition. *Tetrahedron* **2008**, *64*, 11409–11419.

(61) Mahoney, J. M.; Beatty, A. M.; Smith, B. D. Selective Recognition of an Alkali Halide Contact Ion-Pair. *J. Am. Chem. Soc.* **2001**, *123*, 5847–5848.

(62) Li, D.-H.; Smith, B. D. Shape-Selective Recognition of Quaternary Ammonium Chloride Ion Pairs. *J. Org. Chem.* **2019**, *84*, 2808–2816.

(63) Frisch, M. J.; Trucks, G. W.; Schlegel, H. B.; Scuseria, G. E.; Robb, M. A.; Cheeseman, J. R.; Scalmani, G.; Barone, V.; Petersson, G. A.; Nakatsuji, H.; Li, X.; Caricato, M.; Marenich, A. V.; Bloino, J.; Janesko, B. G.; Gomperts, R.; Mennucci, B.; Hratchian, H. P.; Ortiz, J. V.; Izmaylov, A. F.; Sonnenberg, J. L.; Williams-Young, D.; Ding, F.; Lipparini, F.; Egidi, F.; Goings, J.; Peng, B.; Petrone, A.; Henderson, T.; Ranasinghe, D.; Zakrzewski, V. G.; Gao, J.; Rega, N.; Zheng, G.; Liang, W.; Hada, M.; Ehara, M.; Toyota, K.; Fukuda, R.; Hasegawa, J.; Ishida, M.; Nakajima, T.; Honda, Y.; Kitao, O.; Nakai, H.; Vreven, T.; Throssell, K.; Montgomery, J. A., Jr.; Peralta, J. E.; Ogliaro, F.; Bearpark, M. J.; Heyd, J. J.; Brothers, E. N.; Kudin, K. N.; Staroverov, V. N.; Keith, T. A.; Kobayashi, R.; Normand, J.; Raghavachari, K.; Rendell, A. P.; Burant, J. C.; Iyengar, S. S.; Tomasi, J.; Cossi, M.; Millam, J. M.; Klene, M.; Adamo, C.; Cammi, R.; Ochterski, J. W.; Martin, R. L.; Morokuma, K.; Farkas, Ö.; Foresman, J. B.; Fox, D. J. Gaussian 16, Rev. C01.

(64) Zhao, Y.; Truhlar, D. G. The M06 Suite of Density Functionals for Main Group Thermochemistry, Thermochemical Kinetics, Noncovalent Interactions, Excited States, and Transition Elements: Two New Functionals and Systematic Testing of Four M06-Class Functionals and 12 Other Functionals. *Theor. Chem. Acc.* **2008**, *120*, 215–241.

(65) Zhao, Y.; Truhlar, D. G. A New Local Density Functional for Main-Group Thermochemistry, Transition Metal Bonding, Thermochemical Kinetics, and Noncovalent Interactions. *J. Chem. Phys.* **2006**, *125*, 194101.

(66) Zhao, Y.; Truhlar, D. G. Density Functional for Spectroscopy: No Long-Range Self-Interaction Error, Good Performance for Rydberg and Charge-Transfer States, and Better Performance on Average than B3LYP for Ground States. *J. Phys. Chem. A* **2006**, *110*, 13126–13130.

(67) Weigend, F.; Ahlrichs, R. Balanced Basis Sets of Split Valence, Triple Zeta Valence and Quadruple Zeta Valence Quality for H to Rn: Design and Assessment of Accuracy. *Phys. Chem. Chem. Phys.* **2005**, *7*, 3297.

(68) Peterson, K. A.; Figgen, D.; Goll, E.; Stoll, H.; Dolg, M. Systematically Convergent Basis Sets with Relativistic Pseudopotentials. II. Small-Core Pseudopotentials and Correlation Consistent Basis Sets for the Post- *d* Group 16–18 Elements. *J. Chem. Phys.* **2003**, *119*, 11113–11123.

(69) Feller, D. The Role of Databases in Support of Computational Chemistry Calculations. *J. Comput. Chem.* **1996**, *17*, 1571–1586.

(70) Schuchardt, K. L.; Didier, B. T.; Elsethagen, T.; Sun, L.; Gurumoorthi, V.; Chase, J.; Li, J.; Windus, T. L. Basis Set Exchange: A Community Database for Computational Sciences. *J. Chem. Inf. Model.* **2007**, *47*, 1045–1052.

(71) Pritchard, B. P.; Altarawy, D.; Didier, B.; Gibson, T. D.; Windus, T. L. New Basis Set Exchange: An Open, Up-to-Date Resource for the Molecular Sciences Community. *J. Chem. Inf. Model.* **2019**, *59*, 4814–4820.

(72) Wang, H.; Wang, W.; Jin, W. J. σ-Hole Bond vs π-Hole Bond: A Comparison Based on Halogen Bond. *Chem. Rev.* **2016**, *116*, 5072–5104.

(73) The Energy Differences (ΔE298) Were Calculated from the Electronic Energies (*ε*0) Corrected with the Zero-Point Energies (*ε*ZPVE) and the Thermal Energy Corrections (with Contributions from Translation, Vibrational Motion, Rotational Motion and Electronic Motion).

Insert Table of Contents artwork here